J Mater Sci (2008) 43:7057–7065
DOI 10.1007/s10853-008-3063-6

Physical characterization of Y_2O_3–CeO_2–TiO_2 (YCT) mixed oxides and Ni/YCT cermets as anodes in solid oxide fuel cells

X. Mantzouris · G. Triantafyllou · F. Tietz · P. Nikolopoulos

Received: 27 August 2008 / Accepted: 15 October 2008 / Published online: 30 October 2008

Abstract Mixed oxides in the binary Y_2O_3–CeO_2 (YC) and ternary Y_2O_3–CeO_2–TiO_2 (YCT) systems as well as the corresponding Ni cermets were evaluated in terms of application as anodes in solid oxide fuel cells (SOFCs) between 650 and 900 °C. X-ray diffraction (XRD) analysis of the YCT powders calcined up to 1,400 °C showed the cubic fluorite structure of YC and also the formation of an additional phase with pyrochlore structure. The thermal expansion of the ceramics measured in air and Ar/4% H_2 showed no significant differences in the temperature range of 25–800 °C. The absolute values of the total electrical conductivity of the ceramics measured between 450 and 900 °C in Ar/4% H_2 increased by about 1–2 orders of magnitude compared to those measured in air. Ni/$Y_{0.20}Ce_{0.80}O_{1.9}$ and Ni/$Y_{0.20}C_{0.75}Ti_{0.05}O_{1.9}$ cermets with 40 vol% Ni exhibited improved long-term stability regarding their electrical conductivity after annealing at 1,000 °C. The diffusion coefficient of Ce in the 8YSZ electrolyte was measured by compatibility tests. Electrochemical measurements on single SOFCs showed high polarization resistance at the anode/electrolyte interface.

X. Mantzouris · G. Triantafyllou · P. Nikolopoulos (✉)
Department of Chemical Engineering, University of Patras, 26504 Patras, Greece
e-mail: nikolop@chemeng.upatras.gr

F. Tietz
Forschungszentrum Jülich, Institute of Energy Research (IEF-1), 52425 Juelich, Germany

Introduction

Reduction of the operating temperature of solid oxide fuel cells (SOFCs) from 900–1,000 to 650–800 °C is of great importance because it means both prolonged stack lifetime and cost reduction, since the use of low-cost metallic components for interconnects and balance-of-plant materials becomes possible.

For the anode an attractive alternative to the "state of the art" Ni/8YSZ cermet is the use of CeO_2-based materials. The use of ceria in the vicinity of the electrolyte/anode interface has been shown to reduce polarization losses [1, 2]. However, the chemical compatibility between 8YSZ and CeO_2-based materials is not without problems, since the two materials diffuse into each other by preferential migration of Ce ions into the zirconia lattice during the sintering process usually used in SOFC technology [3]. In addition, reduction of Ce^{4+} to Ce^{3+} in the fuel gas atmosphere causes chemical expansion in the CeO_2/8YSZ interdiffusion zone and consequently leads to thermal expansion mismatch and stresses inside the electrolyte due to the larger ionic radius of Ce^{3+} (1.14 Å) compared to Zr^{4+} (0.84 Å) [4]. Partial substitution of CeO_2 by TiO_2 in ceria-based ceramics is expected to suppress the chemical expansion of such ceramic constituents of the anode cermet [5, 6].

In the present work, oxides with the general formula $Y_{0.20}Ce_{0.80-x}Ti_xO_{1.9}$ with x = 0, 0.05, 0.10 and $Y_{0.10}Ce_{0.80}Ti_{0.10}O_{1.95}$ were synthesized and examined with respect to their crystal structure, thermal expansion and electrical conductivity. The long-term stability of the electrical conductivity of the corresponding cermets with 40 vol% Ni as well as the chemical compatibility of NiO-containing ceramics in contact with 8YSZ electrolyte was investigated for their application as anodes in an SOFC. Finally

electrochemical tests were performed on single cells with an anode cermet composed of Ni(40 vol%)/$Y_{0.15}Ce_{0.75}Ti_{0.10}O_{2-x}$.

Experimental

All ceramic compositions were synthesized by co-precipitation with a diluted ammonia solution using the starting materials $Y(NO_3)_3 \cdot 5H_2O$, $Ce(NO_3)_3 \cdot 6H_2O$ and $TiCl_3$ in HCl in the appropriate amounts dissolved in nitric acid. The precipitates were filtered and carefully washed with distilled water until no chloride ions could be detected with a silver nitrate solution. Subsequently the powders were dried overnight at 120 °C and calcined at 700 °C. Parts of the ceramic powders were mixed with the appropriate amounts of NiO (J.T. Baker, >99%) to achieve Ni contents of 40 vol% after reduction at 900 °C in Ar/4% H_2 atmosphere for 5 h. All mixtures were wet-milled with ethanol in a centrifugal ball mill for 50 h for homogenization and reduction of the mean grain size.

For the crystal structure investigations small amounts of the ceramic powders calcined at 700 °C were heated up to 1,400 °C for 5 h in air in steps of 100 °C and subjected to X-ray diffraction (XRD). The experiments were performed at room temperature using a Philips PW 1830/40 diffractometer and Cu K_α radiation.

For the thermal expansion and electrical conductivity measurements, samples of the ceramics and the NiO/YCT mixtures were uniaxially pressed to rectangular bars ($3 \times 3 \times 25$ mm^3) and sintered at 1,400 °C for 5 h in air. The density of the specimens was about 95% of the theoretical density. The thermal expansion measurements were carried out in air and Ar/4% H_2 atmosphere with a push-rod dilatometer 402E from Netzsch (Selb, Germany) in the temperature range of 25–1,000 °C at a heating rate of 3 K/min. Electrical conductivity was measured up to 900 °C using a four-probe DC technique with Ag wires wrapped around the samples. Current and voltage were measured with a Keithley multimeter and automatically recorded using the Test Point software package.

For the chemical compatibility measurements, thick films of a selected NiO/YCT paste were coated on compact 8YSZ pellets made of Tosoh powder, ball-milled for 50 h and sintered at 1,400 °C for 5 h. The paste was prepared by mixing the oxide powders with a binder consisting of 6% ethylcellulose in terpineol. The specimens were sintered at 1,400 °C and different time intervals in air and Ar/4%H_2. The interdiffusion across the anode/electrolyte interface was investigated using SEM-EDS analysis on metallographically prepared cross-sections of the samples.

The electrochemical tests were performed on anode-supported single cells with 8YSZ as electrolyte and LSM as cathode. The integration of Ni/YCT anode layers and the details of the cell tests are described elsewhere [7, 8].

Results and discussion

Crystal structure characterization

X-ray diffraction analysis of the air-calcined powders indicates that $Y_{0.20}Ce_{0.80}O_{1.9}$ (YC) crystallizes in the cubic fluorite-type structure while in the Ti-containing YCT ceramics an additional phase ($Y_2Ti_2O_7$) with cubic pyrochlore structure was formed. Figure 1 presents the diffractograms of the investigated oxides after calcination at 1,400 °C for 5 h as well as the corresponding lattice parameters, α_c, of the cubic fluorite structures. The observed small deviations of the lattice parameter values (Fig. 1) indicate limited solubility of Ti in the fluorite matrix. The calculated value, $\alpha_c = 540.0 \pm 0.3$ pm, for the $Y_{0.20}Ce_{0.80}O_{1.9}$ ceramic lies between the reported values of 540.5 [9] and 539.5 pm [10].

As can be seen from the diffractograms of $Y_{0.20}Ce_{0.70}Ti_{0.10}O_{1.9}$ powder, calcined for 5 h in air between 700 and 1,400 °C in steps of 100 °C (Fig. 2a), the pyrochlore structure appears in a detectable quantity at 900 °C. The ratios of the 100%-intensity peaks of the fluorite to the pyrochlore structure, i.e., (111) at $2\theta = 28.5°$ and (222) at $2\theta = 30.5°$, respectively, decrease with increasing temperature (Fig. 2b), indicating that the higher reaction rate for pyrochlore formation restrains the solubility limit of TiO_2 in the fluorite phase. The same behavior

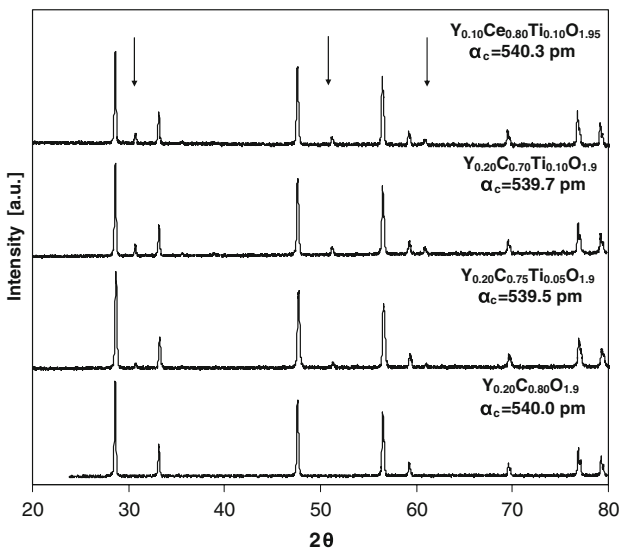

Fig. 1 XRD patterns and lattice parameter, α_c, of the cubic fluorite structure for the YC and YCT ceramics after calcination at 1,400 °C for 5 h in air (arrows indicate the additional peaks of the pyrochlore phase)

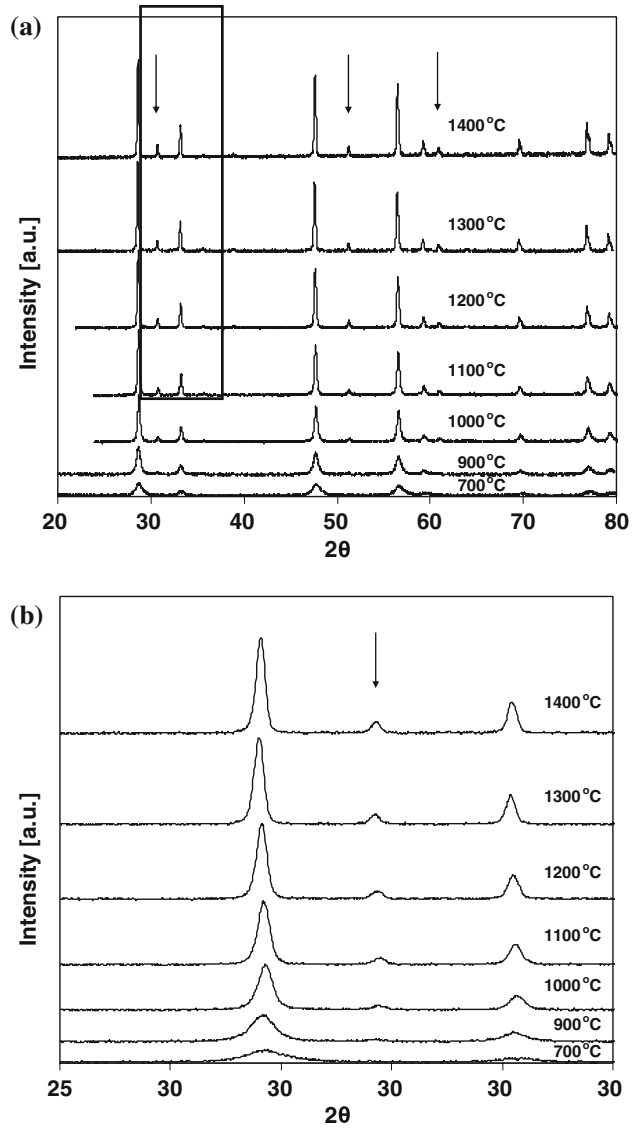

Fig. 2 **a** XRD patterns of $Y_{0.20}Ce_{0.70}Ti_{0.10}O_{1.9}$ powder after calcination for 5 h in air between 700 and 1,400 °C in steps of 100 °C (arrows indicate the additional peaks of the pyrochlore phase). **b** The 100% intensity peaks of fluorite (111) and pyrochlore (222)

was also observed in the diffractograms of the other YCT powders.

Figure 3 shows the temperature dependence of the amount of pyrochlore phase (in wt%) formed in the YCT ceramics, calculated from the ratio of peak areas of the reflections with highest intensity $(111)_{fluorite}$ and $(222)_{pyrochlore}$.

The formation of the pyrochlore phase ($Y_2Ti_2O_7$) results in the alteration of the exact composition of the fluorite phase in the ceramics. In particular, considering the XRD results the composition of the fluorite phase after calcination at 1,400 °C for 5 h in air is $Y_{0.169}Ce_{0.827}Ti_{0.004}O_{1.916}$, $Y_{0.143}Ce_{0.833}Ti_{0.024}O_{1.929}$, and $Y_{0.020}Ce_{0.96}Ti_{0.04}O_{1.99}$ for $Y_{0.20}Ce_{0.75}Ti_{0.05}O_{1.9}$, $Y_{0.20}Ce_{0.70}Ti_{0.10}O_{1.9}$ and $Y_{0.10}Ce_{0.80}Ti_{0.10}O_{1.95}$, respectively. In the case of $Y_{0.20}Ce_{0.70}Ti_{0.10}O_{1.9}$ the above result is supported by SEM-EDS point analysis, which showed that the cubic fluorite structure contains 14.3 ± 0.5 at% Y, 83.0 ± 0.6 at% Ce, and 2.7 ± 0.2 at% Ti. From the lattice parameters of the fluorite phases given in Fig. 1 and for $Y_2Ti_2O_7$ as 1008.0 pm [11], the densities as well as the volume fractions of pyrochlore formed in the YCT ceramics can be calculated. According to these calculations, the $Y_2Ti_2O_7$ content ($\rho_{pyrochlore} = 5.0$ g/cm^3) can be given as 7.7, 13.4, and 13.9 vol% for $Y_{0.20}Ce_{0.75}Ti_{0.05}O_{1.9}$ ($\rho_{fluorite} = 6.84$ g/cm^3), $Y_{0.20}Ce_{0.70}Ti_{0.10}O_{1.9}$ ($\rho_{fluorite} = 6.82$ g/cm^3), and $Y_{0.10}Ce_{0.80}Ti_{0.10}O_{1.95}$ ($\rho_{fluorite} = 7.12$ g/cm^3), respectively.

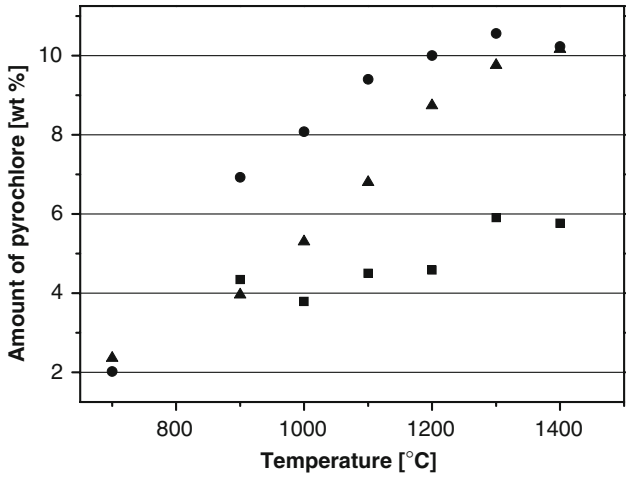

Fig. 3 Temperature dependence of pyrochlore formation (wt%) in the YCT ceramics with nominal compositions: $Y_{0.20}Ce_{0.70}Ti_{0.10}O_{1.9}$ (●), $Y_{0.20}Ce_{0.75}Ti_{0.05}O_{1.9}$ (■), and $Y_{0.10}Ce_{0.80}Ti_{0.10}O_{1.95}$ (▲)

Thermal expansion

The thermal expansion coefficient (TEC) is an important factor in SOFC design. A significant degree of mismatch in TEC values between the anode and the electrolyte can result in large stresses causing cracks in the electrolyte or delamination either during fabrication or under operating conditions.

The TEC values of the tested YC and YCT oxides measured in air between 25 and 1,000 °C (Table 1) were found to be about 20% higher than the corresponding value of 8YSZ (10.5×10^{-6} K^{-1}) [12], showing a slight trend towards smaller values with increasing Ti content. This is due to the smaller TEC of $Y_2Ti_2O_7$ (11.21×10^{-6} K^{-1}) [13]. Comparative measurements on the same oxides in air and Ar/4% H_2 show no significant changes of thermal expansion in the temperature range 25–800 °C, whereas for the cermets with 40 vol% Ni the corresponding values increase by about 15% due to the presence of Ni (Table 1).

In the temperature range of 800–1,000 °C in Ar/4% H_2 the YC and YCT samples revealed considerable

Table 1 TEC values ($\times 10^{-6}$ K^{-1}) of YC and YCT oxides in air and Ar/4% H_2 and of the corresponding Ni cermets with 40 vol% Ni

Nominal composition	TEC/10^{-6} K^{-1} in air (25–1,000 °C)	TEC/10^{-6} K^{-1} in air (25–800 °C)	TEC/10^{-6} K^{-1} in Ar/4% H_2 (25–800 °C)	TEC/10^{-6} K^{-1} in Ar/4% H_2 (25–800 °C) Cermet with 40 vol% Ni
$Y_{0.20}Ce_{0.80}O_{1.9}$	12.6	12.3	12.6	14.8
$Y_{0.20}Ce_{0.75}Ti_{0.05}O_{1.9}$	12.6	12.3	12.5	14.7
$Y_{0.20}Ce_{0.70}Ti_{0.10}O_{1.9}$	12.3	12.0	12.3	14.3
$Y_{0.10}Ce_{0.80}Ti_{0.10}O_{1.95}$	12.4	12.1	12.6	14.9

dimensional changes with increasing TECs (Fig. 4). This behavior is caused by the reduction of Ce^{4+} (r = 0.97 Å) to Ce^{3+} (r = 1.14 Å), which led to a significant degree of chemical expansion at elevated temperatures. Comparing the $Y_{0.10}Ce_{0.80}Ti_{0.10}O_{1.95}$ and $Y_{0.20}Ce_{0.70}Ti_{0.10}O_{1.9}$ samples, with about the same $Y_2Ti_2O_7$ content, the latter composition shows a lower relative expansion (Fig. 4) due to the higher degree of substitution with Y in the fluorite phase. According to the combination of dissolution of Y_2O_3 in CeO_2 (Eq. 1) and the reduction reaction of Ce ions (Eq. 2), the low Y content of the fluorite phase shifts Eq. 2 to the right side resulting in a more reduced system.

$$Y_2O_3 \xrightarrow{CeO_2} 2Y'_{Ce} + 3O^x_O + V^{\cdot\cdot}_O \quad (1)$$

$$2Ce_{Ce} + O_O = 2Ce'_{Ce} + V^{\cdot\cdot}_O + 1/2O_2 \quad (2)$$

Similar results have been reported in the literature for CaO- and Gd_2O_3-containing CeO_2 [14].

A higher $Y_2Ti_2O_7$ concentration in samples with a similar Y content in the fluorite structure also suppresses the chemical expansion.

Electrical conductivity of ceramics

The Arrhenius plots (log (σT) versus 1,000/T) of the total conductivity of the tested ceramics measured in air as well as for 8YSZ [15], are illustrated in Fig. 5. The straight lines obtained in the temperature range of 450–900 °C indicate that the conductivity is almost entirely ionic. This is in accordance with studies which specify that the electrolytic domain ($t_i \geq 0.99$) of Y-substituted ceria exists up to $p(O_2) = 10^{-13}$ bar at 600 °C and $p(O_2) = 10^{-4}$ bar at 900 °C [16]. Table 2 includes the conductivity values at 800 °C and the corresponding activation energy in the range of 450–900 °C.

The ionic conductivity values of the ceramics containing 20 mol% $YO_{1.5}$ ($Y_{0.20}Ce_{0.80-x}Ti_xO_{1.9}$) are higher than those of 8YSZ in the whole temperature range examined and decrease with increasing Ti content. The lowering of the conductivity can be attributed on the one hand to the substitution of small amounts of CeO_2 with TiO_2 and the associated trapping of oxygen ions in the vicinity of Ti ions. On the other hand, the main factor leading to the

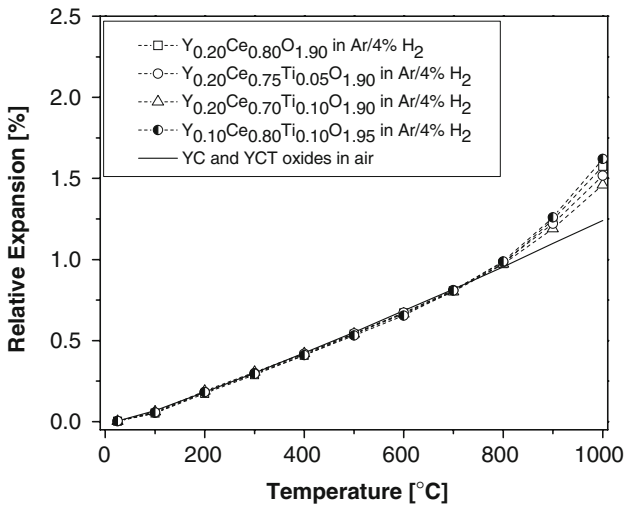

Fig. 4 Relative thermal expansion of YC and YCT ceramics in air and Ar/4% H_2 atmosphere between 25 and 1,000 °C

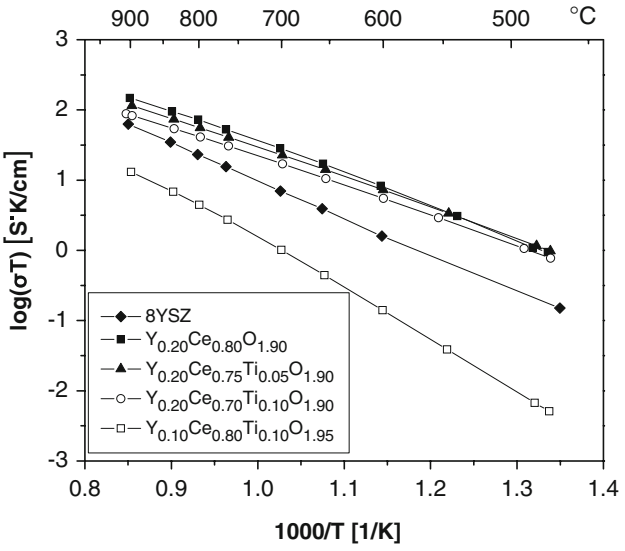

Fig. 5 Arrhenius plots of the total electrical conductivity of YC and YCT ceramics as well as of 8YSZ [15] measured between 450 and 900 °C in air

Table 2 Ionic conductivity at 800 °C, $\sigma_{800\ °C}$, of YC and YCT oxides as well as of 8YSZ [15] measured in air, and the corresponding activation energies, E_a, between 450 and 900 °C

Nominal composition	$\sigma_{800\ °C}$ (mS cm^{-1})	E_a (eV)
$Y_{0.20}Ce_{0.80}O_{1.9}$	62.9	0.91
$Y_{0.20}Ce_{0.75}Ti_{0.05}O_{1.9}$	51.8	0.85
$Y_{0.20}Ce_{0.70}Ti_{0.10}O_{1.9}$	38.4	0.85
$Y_{0.10}Ce_{0.80}Ti_{0.10}O_{1.95}$	4.18	1.42
8YSZ	21.6	1.05

decrease of conductivity is the increasing amount of the low-conductive $Y_2Ti_2O_7$ phase [11, 17], which induces a reduction of the concentration of charge carriers (oxygen vacancies). This assumption is confirmed by the significant drop of the ionic conductivity observed for the YCT ceramic containing 10 mol% $YO_{1.5}$ with an activation energy of 1.42 eV (Table 2), which approaches the corresponding values for pure CeO_2 (1.70 eV) [18]. The conductivity of 62.9 mS/cm for $Y_{0.20}Ce_{0.80}O_{1.9}$ at 800 °C lies in the range of values (62.3–78.2 mS/cm) reported in the literature [9, 19–22], for highly dense samples (>95% of the theoretical density) and is about three times higher than the corresponding value (21.6 mS/cm) for 8YSZ (Table 2). The activation energy of $E_a = 0.91$ eV between 450 and 900 °C agrees well with the value between 250 and 850 °C given by Zhang et al. (0.931 eV) [9].

The influence of Ti content in the YCT ceramics is illustrated in Fig. 6 together with Ti-free ceria materials. Without Ti, the yttria- and gadolinia-substituted cerias show a maximum ionic conductivity at an oxygen vacancy concentration, $c(V_O^{\cdot\cdot})$, of 10%, i.e., a substitution level of 20% Y [9, 19–21] or Gd [23]. At higher or lower $c(V_O^{\cdot\cdot})$, the conductivity decreases nearly linearly with similar slope. In the case of the materials investigated here, $Y_{0.20}Ce_{0.80}O_{1.9}$ showed the highest conductivity as reported previously [9, 23]. The addition of Ti not only changes $c(V_O^{\cdot\cdot})$ due to the formation of $Y_2Ti_2O_7$, it also decreases the conductivity to a larger extent than expected. Therefore an additional influence of the Ti ions acts as a barrier for ionic conduction. Since the three data points of the YCT ceramics give a straight line with a different slope than that for the Ti-free values it can be assumed that the mobility of the oxygen vacancies is affected either by trapping of oxygen in the vicinity of Ti ions or around the $Y_2Ti_2O_7$ grains.

In Ar/4% H_2 atmosphere the conductivity increases and the activation energy significantly decreases at lower temperatures compared to the corresponding values in air indicating mixed ionic-electronic conduction (Fig. 7). This is attributed to the reduction of Ce^{4+} and Ti^{4+} to Ce^{3+} and Ti^{3+}, respectively, which leads to an additional electronic n-type conductivity. The resulting smaller activation

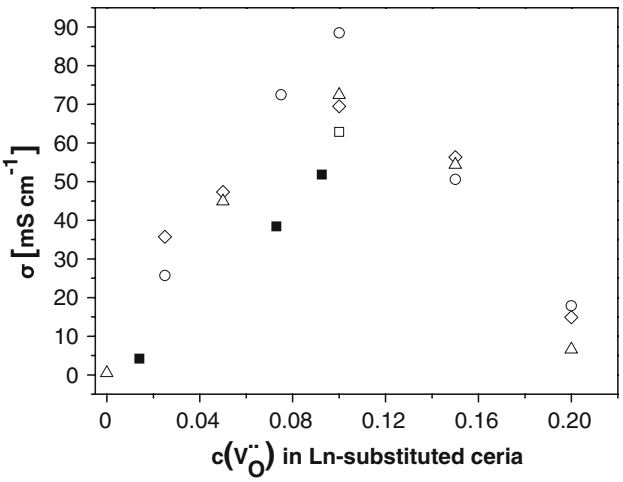

Fig. 6 Dependence of ionic conductivity at 800 °C on oxygen vacancy concentration for ceria with different lanthanide substitutions: $Ce_{1-x}Y_xO_{2-x/2}$ (◇) [9], $Ce_{1-x}Y_xO_{2-x/2}$ (Δ) [19, 21], $Ce_{1-x}Gd_xO_{2-x/2}$ (○) [23], YC (□), and YCT (■), this work

energy under reducing conditions compared to the values in air arises from the lower value of the activation energy of electron hopping in ceria solid solutions [24, 25]. From the results it is deduced that replacing CeO_2 with small amounts of TiO_2 in $Y_{0.20}Ce_{0.80-x}Ti_xO_{1.9}$ does not significantly influence the electrical conductivity at high temperatures. The electronic contribution to the total electrical conductivity is more pronounced in the $Y_{0.10}Ce_{0.80}Ti_{0.10}O_{1.95}$ system. The reduced yttria concentration in the fluorite phase suppresses the electrolytic domain by increasing the electronic contribution to the conductivity compared to $Y_{0.20}Ce_{0.80-x}Ti_xO_{1.9}$ systems. Similar results have been published by Levy et al. [25] for nonstoichiometric Y-doped ceria solid solutions, while the same trend is valid for Ca- and Gd-doped ceria systems [26, 27].

Electrical conductivity of Ni/YC and Ni/YCT cermets with 40 vol% Ni

The temperature dependence of the electrical conductivity of the cermets exhibited a metallic character. The long-term stability of the electrical conductivity of the Ni/YC and Ni/YCT cermets was examined after exposure at 1,000 °C in flowing Ar/4% H_2 atmosphere for up to 1,000 h. At fixed time intervals the annealing was interrupted and the electrical conductivity of the samples was measured in the temperature range of 25–900 °C.

Figure 8 illustrates the conductivity results at 800 °C as a function of the exposure time. The scatter in electrical conductivity values appearing at the beginning of the experiments between the samples is attributed to the difference in porosity reflecting the final stage of cermet

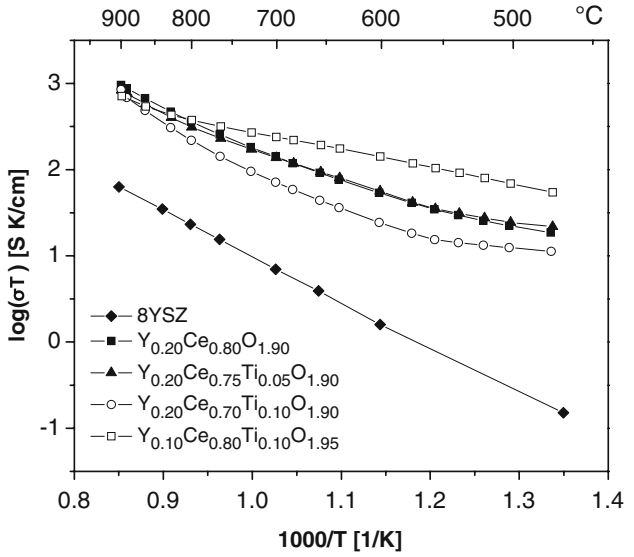

Fig. 7 Arrhenius plots of the total electrical conductivity of YC and YCT ceramics as well as of 8YSZ [15] measured between 450 and 900 °C in Ar/4% H_2

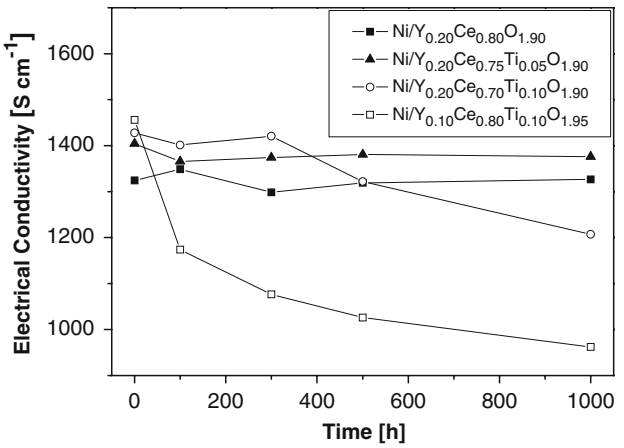

Fig. 8 Electrical conductivity at 800 °C of Ni/YC and Ni/YCT cermets with 40 vol% Ni as a function of the annealing time at 1,000 °C in Ar/4% H_2 atmosphere

preparation as well as to the structure configuration of the metal network.

A significant parameter for the evaluation of the cermet stability after long-term annealing is the difference between the initial (0 h) and the final (1,000 h) electrical conductivity values. The results (Fig. 8) show that for cermets with high yttria and low titania content in the ceramic phase the conductivity values remain practically constant during annealing, whereas for low yttria and high titania content the conductivity decreases significantly. This behavior can be explained in terms of interfacial interactions established at the metal/ceramic interface of the cermet [28, 29].

Wetting experiments in systems of liquid Ni in contact with different ceramics, including pure CeO_2 performed at 1,500 °C in Ar/4% H_2 atmosphere resulted in contact angle θ values equal to 114°, 110°, 103°, 99°, and 96° for the systems $Ni/Y_{0.2}Ce_{0.8}O_{1.9}$, CeO_2, $Y_{0.2}Ce_{0.75}Ti_{0.05}O_{1.9}$, $Y_{0.20}Ce_{0.70}Ti_{0.10}O_{1.90}$, and $Y_{0.10}Ce_{0.80}Ti_{0.10}O_{1.95}$, respectively (Fig. 9).

The systems $Ni/Y_{0.2}Ce_{0.8}O_{1.9}$ and Ni/CeO_2 are nonwetted and nonreactive ($\theta \geq 110^o$) with limited solubility of the ceramic phase in the liquid metal [28, 30]. Addition of 20 mol% $YO_{1.5}$ of the high surface energy Yttria in ceria increases the contact angle compared to pure CeO_2, enhances simultaneously the resistance to reduction of the ceramic [14, 31].

In the case of the Ni/YCT systems, the observed lower contact angle values are attributed to the enrichment of the interface with titania-containing pyrochlore phase, as revealed by SEM observations of sample cross-sections. Furthermore, the high amounts of TiO_2 suppress the substituents content in the fluorite phase of the ceramics and therefore their reduction resistance. The investigated

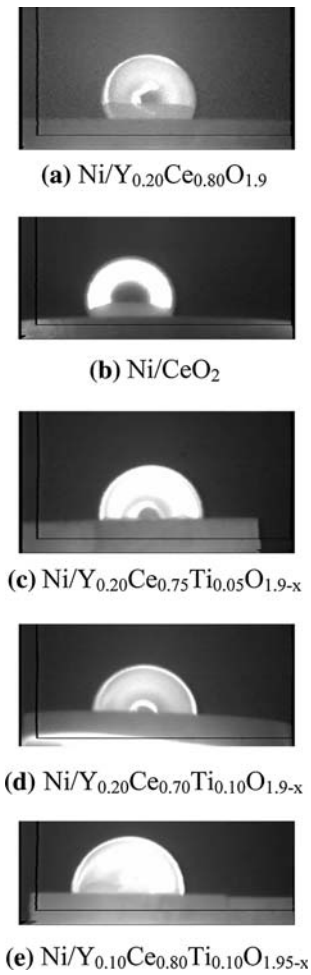

Fig. 9 Sessile drop of liquid Ni on YC- and YCT-ceramics substrates at 1,500 °C in Ar/4% H_2

Ni/YCT systems are nonwetted. However the decreasing contact angle values far below $\theta = 110^{o}$, indicate that a reaction can be established across the metal-ceramic interface even if this could not be proven in SEM-EDS investigations.

For the long-term annealing experiments at 1,000 °C the interfacial reaction is the possible reason for decreasing with time of the electrical conductivity of the anode cermets, with high TiO_2 content (10 mol% TiO_2) in the ceramic phase (Fig. 8). SOFC operation at reduced temperatures is expected to diminish this phenomena as well as deviation from stoichiometry.

Chemical compatibility

High-temperature sintering for preparation and long-term SOFC operation causes a cation interdiffusion zone at the anode/electrolyte interface leading to the deterioration of the cell performance [32, 33].

In the case of a layered sample of $Y_{0.20}Ce_{0.75}Ti_{0.05}O_{1.9}$ (YCT) + NiO/8YSZ, sintered at 1,400 °C for 5 h in air, the EDS line scanning (Fig. 10) across the anode/electrolyte interface shows the formation of an interdiffusion zone. Emerging porosity can be recognized on the YCT + NiO side resulting from the difference in diffusion coefficients of the counter-diffusing cations (Ce^{4+} in 8YSZ and Zr^{4+} in YCT + NiO) causing Kirkendahl voids.

The results of SEM point analysis show high diffusivity of Ce^{4+} in 8YSZ, while the corresponding migration of Zr^{4+} is significantly lower. Figure 11 presents the compositional distribution of Ce^{4+} in 8YSZ electrolyte for different annealing times up to 50 h. In the same analysis, after 50 h of sintering Zr^{4+} appeared in the YCT + NiO region in a detectable quantity at a depth of 2 μm from the interface with an atomic concentration of about 1.5 at%. Sintering of $Y_{0.20}Ce_{0.75}Ti_{0.05}O_{1.9}$ (YCT) + NiO/8YSZ samples at 1,400 °C for 50 h in Ar/4% H_2 revealed reduced diffusivity of cerium ions through the 8YSZ electrolyte (Fig. 11) due to the reduction of Ce^{4+} to Ce^{3+} with larger ionic radius. Additional experiments performed on sintered NiO + YCT/8YSZ samples at 1,400 °C for 5 h in air and following exposure at 900 °C for 200 h in Ar/4% H_2 showed no shift of the diffusion curves of Ce ions towards higher depths.

The effective Ce^{4+} diffusion coefficient, D_{eff}, (bulk + grain boundary diffusion) in 8YSZ at 1,400 °C in air (Fig. 11) was determined using the solution of Fick's law for low diffusion times and semi-infinite space:

$$\frac{c(x,t)}{c_0} = \exp\left(-\frac{x^2}{4D_{\text{eff}}t}\right) \tag{3}$$

The calculated value $D_{\text{eff}} = 1.9 \times 10^{-17}$ m^2/s at 1,400 °C differs by more than one order of magnitude compared to the value of 0.83×10^{-18} m^2/s reported by Bekale et al. [34], for Gd-doped ceria samples in contact

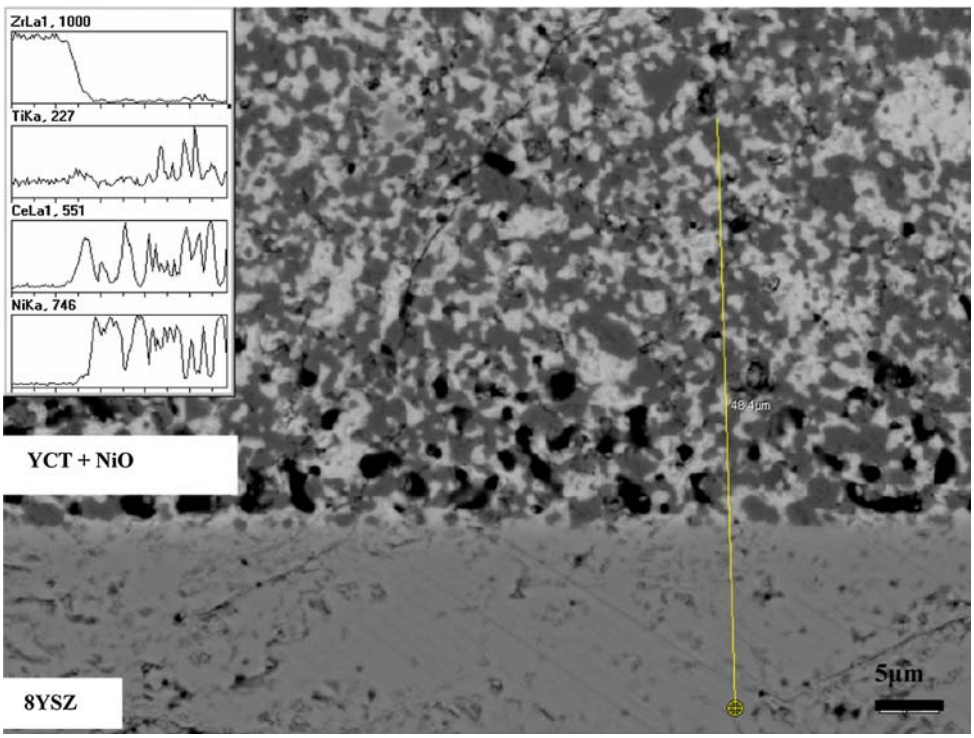

Fig. 10 Line scan across the YCT + NiO/8YSZ interface after sintering at 1,400 °C for 5 h in air

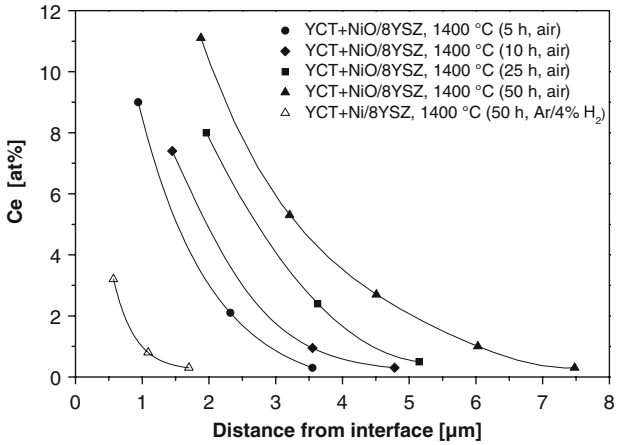

Fig. 11 Diffusivity of Ce ions in the 8YSZ electrolyte across the YCT + NiO/8YSZ interface, sintered at 1,400 °C in air for different times (closed symbols) as well as in Ar/4% H_2 for 50 h (open symbols)

with highly dense 8YSZ (99.5% of theoretical density), under the same experimental conditions. This difference can be attributed to the smaller grain size ($\phi = 1.5$ µm) of 8YSZ used in this work resulting in a stronger influence of grain boundary diffusion on the effective diffusion, as well as to the higher porosity (95% of theoretical density) of the samples. The effective diffusion coefficient D_{eff} can be correlated with the bulk diffusion coefficient, D_{b}, and the grain boundary diffusion coefficient, D_{gb}, through the relationship [34].

$$D_{\text{eff}} = (1 - f)D_{\text{b}} + f\alpha D_{\text{gb}} \tag{4}$$

where, α is the segregation factor, $f = 3\delta/\phi$ is the fraction of atomic sites located on the grain boundaries, δ is the grain boundary width, and ϕ represents the grain size. Assuming a diffusion coefficient ratio $D_{\text{gb}}/D_{\text{b}} = 0.26531 \times 10^5$ at 1,400 °C given by Bekale et al. [34] and for $\alpha = 1$, $\delta = 1$ nm and $\phi = 1.5$ µm, it follows from Eq. 4 $D_{\text{b}} = 3.5 \times 10^{-19}$ m^2/s and $D_{\text{gb}} = 9.3 \times 10^{-15}$ m^2/s.

Cell manufacturing and electrochemical tests

The possible use of Ni/YCT cermets as anode materials was evaluated in anode-supported SOFCs. For this purpose, five YCT materials were used as ceramics in composites with 40 vol% Ni and eight single cells were manufactured for each YCT material, 90% of these cells showed a He leakage rate of more than 8×10^{-4} mbar l cm^{-2} s^{-1} applying a pressure difference of 100 mbar as under stack operating conditions. The lowest He leakage rate was 3.1×10^{-4} mbar l cm^{-2} s^{-1}. This means that all the cells had a higher leakage rate than the internal quality control threshold at Forschungszentrum Jülich. Despite this fact, two single cells with Ni/$Y_{0.15}Ce_{0.75}Ti_{0.10}O_{2-x}$ anode

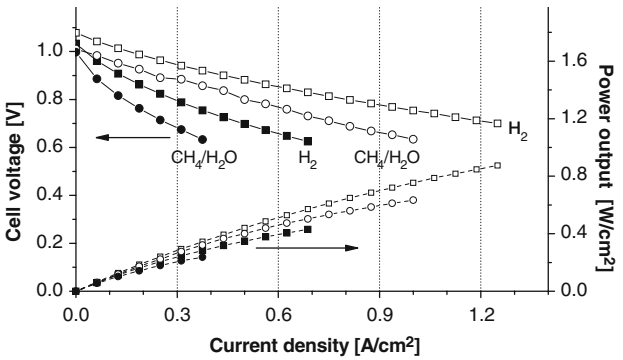

Fig. 12 Current-voltage curves for 5 × 5 cm^2 anode-supported single cells with Ni(40 vol%)/$Y_{0.15}Ce_{0.75}Ti_{0.10}O_{2-x}$ and Ni(40 vol%)/8YSZ anodes at 800 °C. For the cell tests 1,000 mL/min air as oxidant and either 1,000 mL/min H_2 with 3% H_2O or 330 mL/min CH_4 with 670 mL/min H_2O as fuel gas was supplied to the cells

functional layer were tested together with cells containing the "state of the art" Ni/8YSZ anodes. The anode substrate, electrolyte and cathode were fabricated in the same batch to guarantee a reliable comparison of the cell test results.

Figure 12 illustrates the current-voltage curves of 5 × 5 cm^2 cells with Ni/$Y_{0.15}Ce_{0.75}Ti_{0.10}O_{2-x}$ anode at 800 °C as well as the corresponding data of a cell with Ni/8YSZ anode for H_2/3% H_2O and 33% CH_4/67% H_2O as fuel gases.

The obviously poorer performance of the SOFC with the Ni/YCT anode can be mainly attributed to the higher gas leakage as indicated by the lower open circuit potential but also to the higher polarization resistance. The latter increases due to the presence of the gas leakage, because of the partial deterioration of the cathode due to the penetrating fuel gas [35]. After the cell test, several small areas of the cathode were detached from the electrolyte. The reason for the higher gas leakage may be related, at least partly, to the diffusion of Ce^{4+} into the 8YSZ electrolyte. In an SEM investigation after the cell test, no obvious defects or increased porosity in the electrolyte was observed. The only difference compared to the conventional 8YSZ electrolyte was a more facetted instead of a smooth fracture surface.

Conclusions

YC and YCT ceramics as well as the corresponding Ni-cermets were synthesized and investigated with regard to their physical properties. The results showed: (a) limited solubility of Ti in the fluorite lattice of YC, while higher amounts of TiO_2 lead to the formation of $Y_2Ti_2O_7$ with pyrochlore structure suppressing the thermal expansion of the ceramic, (b) the electrical conductivity of the high yttria- and low titania-containing ceramics in air is higher

than that of 8YSZ and increases significantly in Ar/4% H_2 due to the electronic contribution, (c) Ni cermets with high yttria- and low titania-containing ceramic phase showed excellent long-term stability of the electrical conductivity, (d) the effective diffusion coefficient of Ce^{4+} in the 8YSZ electrolyte was calculated as $D_{eff} = 1.9 \times 10^{-17}$ m^2/s at 1,400 °C in air, and (e) electrochemical tests on single cells showed that the higher gas leakage through the electrolyte is the main reason for the poorer performance of the Ni/YSZ anode. More work is necessary to integrate ceria-based anodes into anode-supported SOFCs.

Acknowledgement Financial support from the European Commission within the EU Integrated Project REALSOFC (Project No. SES6-CT-2003-50261) is gratefully acknowledged.

References

1. Uchida H, Suzuki H, Watanabe M (1998) J Electrochem Soc 145:615
2. Marina OA, Primdahl S, Bagger C, Mogensen M (1997) In: Stimming U et al (eds) Proceedings of the 5th International Symposium on SOFC, The Electrochemical Society, vol 18, p 540
3. Mitsuyasu H, Nonaka Y, Eguchi K (1998) Solid State Ionics 113–115:279
4. Shannon RD (1976) Acta Crystalogr A32:751
5. Tietz F, Jungen W, Lersch P, Figaj M, Becker KD, Skarmoutsos D (2002) Chem Mater 14:2252
6. Armstrong TR, Stevenson JW, Pederson LR, Raney PE (1996) J Electrochem Soc 143:2919
7. Mantzouris X, Zouvelou N, Haanappel VAC, Tietz F, Nikolopoulos P (2007) J Mater Sci 42:10152. doi:10.1007/s10853-007-2099-3
8. Mertens J, Haanappel VAC, Tropartz C, Herzhof W, Buchkremer HP (2006) J Fuel Cell Sci Technol 3:125
9. Zhang TS, Ma J, Huang HT, Hing P, Xia ZT, Chan SH, Kilner JA (2003) Solid State Sci 5:1505
10. Longo V, Podda L (1981) J Mater Sci Lett 16:839
11. Uematsu K, Shinozaki K, Sakurai O, Mizutani N, Kato M (1979) J Am Ceram Soc 62:219
12. Skarmoutsos D, Tietz F, Nikolopoulos P (2001) Fuel Cells 1:243
13. Sigalovsky J, Haggerty J, Sheehan J, Reynolds G (1996) Ceram Eng Sci Proc 17:322
14. Mogensen G, Mogensen M (1993) Thermochim Acta 214:47
15. Skarmoutsos D, Nikolopoulos P, Tietz F, Vinke IC (2004) Solid State Ionics 170:153
16. Tuller HL, Nowick AS (1975) J Electrochem Soc 122:255
17. Yamaguchi S, Kobayashi K, Abe K, Yamazaki S, Iguchi Y (1998) Solid State Ionics 113–115:393
18. Yahiro H, Eguchi K, Arai H (1986) Solid State Ionics 21:37
19. Eguchi K, Setoguchi T, Inoue T, Arai H (1992) Solid State Ionics 52:165
20. Yahiro H, Baba Y, Eguchi K, Arai H (1988) J Electrochem Soc 135:2077
21. Van Herle J, Horita T, Kawada T, Sakai N, Yokokawa H, Dokiya M (1996) Solid State Ionics 86–88:1255
22. Peng R, Xia C, Liu X, Peng D, Meng G (2002) Solid State Ionics 152–153:561
23. Tianshu Z, Hing P, Huang H, Kilner J (2002) Solid State Ionics 148:567
24. Tuller HL, Nowick AS (1977) J Phys Chem Solids 38:859
25. Levy M, Fouletier J, Kleitz M (1980) J de Physique Colloque C6 41:335
26. Arai H, Kunisaki T, Shimizu Y, Seiyama T (1986) Solid State Ionics 20:241
27. Wang S, Kobayashi T, Dokiya M, Hashimoto T (2000) J Electrochem Soc 147:3606
28. Zouvelou N, Mantzouris X, Nikolopoulos P (2007) Int J Adhes Adhes 27:380
29. Mantzouris X, Zouvelou N, Skarmoutsos D, Nikolopoulos P, Tietz F (2005) J Mater Sci 40:2471. doi:10.1007/s10853-005-1977-9
30. Eustathopoulos N, Drevet B (1998) Mater Sci Eng A249:176
31. Mogensen M, Lindegaard T, Hansen UR, Mogensen G (1994) J Electrochem Soc 141:2122
32. Tsoga A, Naoumidis A, Stöver D (2000) Solid State Ionics 135:403
33. Mai A, Haanappel VAC, Tietz F, Stöver D (2006) Solid State Ionics 177:2103
34. Bekale VM, Legros C, Sattonnay G, Huntz AM, Lesage B, Argirusis C, Jomard F (2006) Defect Diffus Forum 258–260:46
35. Tietz F, Wessel E (2002) In: Huijsmans J (ed) Proceedings of the 5th European SOFC Forum, European Fuel Cell Forum, Oberrohrdorf, Switzerland, vol 2, p 814